International Journal of Nanomedicine

Dovepress
open access to scientific and medical research

Open Access Full Text Article

ORIGINAL RESEARCH

Enhancement of osseointegration of polyethylene terephthalate artificial ligament by coating of silk fibroin and depositing of hydroxyapatite

This article was published in the following Dove Press journal:
International Journal of Nanomedicine
29 September 2014
Number of times this article has been viewed

Jia Jiang[1,2]
Fang Wan[1]
Jianjun Yang[1]
Wei Hao[3]
Yaxian Wang[3]
Jinrong Yao[3]
Zhengzhong Shao[3]
Peng Zhang[1]
Jun Chen[1]
Liang Zhou[4]
Shiyi Chen[1]

[1]Fudan University Sports Medicine Center and Department of Sports Medicine and Arthroscopy Surgery, Huashan Hospital, [2]State Key Laboratory of Molecular Engineering of Polymers, [3]Laboratory of Advanced Materials, National Key Laboratory of Molecular Engineering of Polymers, Department of Macromolecular Science, Fudan University, Shanghai, People's Republic of China; [4]Department of Forest Products, Anhui Agricultural University, Hefei Anhui Province, People's Republic of China

Correspondence: Shiyi Chen
Fudan University Sports Medicine Center and Department of Sports Medicine and Arthroscopy Surgery, Huashan Hospital, 12 Middle Wulumuqi Road, Shanghai, 200040, People's Republic of China
Tel +86 21 5288 8255
Fax +86 21 6249 6020
Email cshiyi@163.com

Background: Application of artificial ligament in anterior cruciate ligament reconstruction is one of the research focuses of sports medicine but the biological tendon–bone healing still remains a problem. The preliminary study of hydroxyapatite (HAP) coating on the polyethylene terephthalate (PET) surface could effectively induce the osteoblast differentiation, but the tendon–bone healing was still not stable. As a green synthesis process, the biomimetic mineralization can simulate the natural bone growth in vitro and in vivo.

Methods: HAP crystals were grown under the guide of silk fibroin (SF) PET surface by biomimetic route. Several techniques including scanning electron microscopy, attenuated total reflectance Fourier transform infrared spectroscopy, X-ray diffraction, and energy-dispersive X-ray spectroscopy were utilized for proving the introduction of both SF and HAP. The viability and osseointegration of bone marrow stromal cells on the surface of three kinds of ligament, including PET group (non-coating group), PET+SF group (SF-coating group), and PET+SF+HAP group (combined HAP- and SF-coating group), were analyzed by CCK-8 assays and alkaline phosphatase (ALP) detection. Seventy-two mature male New Zealand rabbits were randomly divided into three groups. Among them, 36 rabbits were sacrificed for mechanical testing, and histological examination for the others.

Results: The SF and SF+HAP were successfully coated on the surface of PET fiber. The CCK-8 assay showed that the cell proliferation on PET+SF+HAP group was better than the other two groups from 24 to 120 hours. After 14 days of culture, the cells in the PET+SF+HAP group delivered higher levels of ALP than the other two groups. After 3 days of culture, the expression level of integrin β1 in the PET+SF+HAP group and PET+SF group were higher than in the PET group. The mean load to failure and the stiffness value of the PET+SF+HAP group were both higher than the other two groups. Hematoxylin and eosin staining showed that new bone tissue formation was only found in the PET+SF+HAP group 8 weeks postoperatively. Masson staining showed that in the PET+SF+HAP group 8 weeks postoperatively, the PET fibers were almost completely encircled by collagen. Histomorphometric analysis showed that the width of the graft–bone interface in the PET+SF+HAP group was narrower than that in the other two groups 4 and 8 weeks postoperatively. The mRNA level of *BMP-7* in the PET+SF+HAP groups was significantly higher than those in the other two groups 4 and 8 weeks postoperatively.

Conclusion: The study showed that the combined SF and HAP coating by biomimetic route on the surface of PET artificial ligament could induce graft osseointegration in the bone tunnel, providing theoretical and experimental foundation for manufacturing novel artificial ligaments meeting the clinical needs.

Keywords: biomineralization, tendon–bone healing, ligament reconstruction

Introduction

The anterior cruciate ligament (ACL) is the most frequently disrupted ligament in the knee joint by providing stability and guiding motion. ACL is frequently injured in athletic maneuvers and accidents.[1,2] It is reported that nearly 95,000 ACL reconstructions are carried out each year in the United States,[3] and most often use biological grafts (autografts and allografts). However, there are several side-effects, such as donor site injury or immunological reaction, of both kinds of grafts.[4–9] Artificial ligaments represent a promising solution to treat ACL injuries without many of the undesirable side effects of autografts and allografts. For example, artificial ligaments such as the Ligament Advanced Reinforcement System (LARS; Surgical Implants and Devices, Arcsur-Tille, France) ligament, made of polyethylene terephthalate (PET) material, have been successfully used in clinical application.[10] In addition, we observed that an interposed layer of fibrous scar tissue appeared at the interface between the graft and bone tunnel in 156 cases of ACL reconstruction using the LARS artificial ligament graft.[11] Like many polymeric or metallic implants, LARS ligaments can cause serious side effects such as severe synovitis.[12,13]

Coating with organic materials of good biocompatibility on artificial graft surface has received increasing interest as an alternative option. In our previous work, hydroxyapatite (HAP) and bioglass coating on PET artificial ligaments could promote the cell compatibility of grafts.[14–16] As a fibrous protein, silk fibroin (SF) from *Bombyx mori* has been used as biomedical material due to its unique structure, biocompatibility, biodegradability, and minimal inflammatory reaction.[17–19] However, it still has problematic characteristics for further clinical applications and use in industrial processes, such as low stiffness and high production cost.[20,21] For this reason, several attempts have been made to improve the properties of silk biomaterials, and this field has become a rapidly growing area of biomaterial research.[22–24] Research has demonstrated that the main inorganic component of human bone tissues, HAP, enhances the compressive strength of silk biomaterials and also induces new bone formation. Therefore, the HAP+SF coating is an attractive candidate for effective surface coating of orthopedic implants and has thus been widely studied in the last decade.[25,26]

Here, we modified the surface of PET artificial ligament by coating with SF and further HAP deposition on it through biomineralization process. Advantages of HAP+SF coating on PET artificial ligament were tested and characterized for its potential in osteoregenerative applications.

Materials and methods

Preparation of the SF solution

Silk fibroin was prepared by the degumming and dissolving of *Bombyx mori* silkworm silk according to established procedures,[27] during which time the silk cocoon was treated with 5% (w/w) Na_2CO_3 boiling solution for 45 minutes to remove sericin; the degummed silk was then dissolved in 9.3 mol/L LiBr aqueous solution. After being filtered, the SF solution was dialyzed against deionized water for 72 hours at room temperature with a 12,000–14,000 molecular weight cutoff dialysis membrane to remove the salt. The dialyzed solution was then clarified by spinning in a centrifuge at 6,000 rpm for about 5 minutes. The supernatant, which was an aqueous regenerated SF solution with concentration of around 2% (w/w), was collected and carefully stored at 4°C.

Pretreatment on the PET ligament

PET sheets (about 10 mm ×10 mm) were taken from a LARS ligament (Surgical Implants and Devices, Arcsur-Tille, France). They were cleaned in the 75% (v/v) alcohol solution for 4 hours, and then washed with a large amount of deionized water. The PET sheets were modified through plasma surface modification (HPD-100B Plasma Apparatus; Coronalab Co., Ltd., Nanjing, People's Republic of China) at 70 V for 40 seconds.

Coating of SF and depositing of HAP on PET ligament

The plasma-treated PET ligaments were immersed in 2% SF solution (made by phosphate-buffered saline [PBS], pH =7.5) at 4°C for 12 hours to form the SF-coated PET. Then, the samples were rinsed with PBS (pH =7.5) and vacuum dried at room temperature. Finally, the PET ligament with SF coating was immersed in the 80% (v/v) ethanol for 2 hours to further fix the SF coating, and then vacuum dried at room temperature for 24 hours. The obtained samples were named as PET+SF.

HAP was deposited onto the PET+SF ligament using an alternate soaking process.[28] In brief, the ligament was immersed in 200 mM $CaCl_2$ solution in a Petri dish placed on a mechanical shaker, with shaking at 150 rpm for 1 hour at 37°C. The ligament was then blotted onto filter paper to remove excess moisture and then immersed in a 120 mM Na_2HPO_4 solution for 1 hour. After soaking alternately for three cycles, the ligament was washed in distilled water and air-dried at room temperature for 24 hours and named as PET+SF+HAP. The non-treated PET sheets, PET+SF sheets and PET+SF+HAP sheets were sterilized through a conventional gas sterilization

technique using ethylene oxide gas prior to in vitro tests or in vivo implantations.

Characterization of three different ligament samples

All three samples, namely PET, PET+SF, and PET+SF+HAP, were observed by scanning electron microscope (SEM) (Tescan TS5136MM; Brno, Czech Republic) at 20 kV accelerating voltage after gold spouting to observe the surface morphology. The crystallization pattern of PET+SF+HAP was recorded on a wide-angle X-ray diffraction (XRD) instrument (D8 Advance; Bruker AXS, Karlsruhe, Germany) with CuKα radiation (λ=0.154 nm). XRD data were collected from 2θ=5 to 70 at a scanning rate of 2°/min. Energy-dispersive X-ray spectroscopy (EDX; Bruker Quantax, Karlsruhe, Germany) analysis (20 kV accelerator voltage) was used to determine the composition, the value of which was averaged from ten tests of the investigated sample. Attenuated total reflectance Fourier transform infrared (ATR-FTIR) measurement was carried out using a Nicolet Nexus 6,700 spectrometer. Each spectrum was recorded with 64 scans and 4.0 cm^{-1} resolution. The spectra of virgin and surface-modified PET films were analyzed in the range of 650–4,000 cm^{-1}. All three samples were adhered to a magnetic steel disc (serving as sample holder) respectively for atomic force microscopy (AFM) measurements. Imaging was recorded on a Nanoscope IV Digital Instruments atomic force microscope (Veeco Metrology Group, Plainview, NY, USA) in tapping mode. In each case, an area of 5×5 μm^2 was scanned, and all images were fitted to a plane using the first-degree flattening procedure enclosed in NanoScope software version 6.12r1.

Cell isolation, seeding, and culturing onto ligaments

Bone marrow stromal cells (BMSCs) were isolated from five New Zealand White rabbits (average weight, 2.5 kg) according to procedures described previously,[29] and cultured in Dulbecco's Modified Eagle's Medium (DMEM) at 37°C in an incubator with 5% CO_2. Three kinds of ligaments were seeded with BMSCs at a density of 7.8×10^4 cell/cm^2.

Cell proliferation, differentiation, and adhesion

BMSC proliferation was measured by cell counting kit-8 (CCK-8) assays as reported previously.[30] BMSCs were seeded on the three kinds of samples (namely PET, PET+SF, and PET+SF+HAP) in 24-well plates and cultured under normal conditions. After 8 hours of culture, the samples were moved to a new culture plate and continued culturing, then cells at different time points (1, 2, 3, 4, and 5 days) were added with 10 μL CCK-8 solution (Dojindo, Tokyo, Kumamoto, Japan) to each well, and cultured for another 4 hours. Then, 100 μL of the supernatants were transferred to a 96-well plate. The absorbance of each specimen was measured at 450 nm using a microplate reader (MultiSkan FC; Waltham, MA, USA). Meanwhile, BMSCs at log growth phase were trypsinized and counted with a hemocytometer for vital cells. The standard curve was established according to the protocol of the kit, and the absorbance at 450 nm (absorbance of each sample – absorbance of sample without cells) was used to calculate the corresponding cell number. All experiments were performed in triplicate.

Alkaline phosphatase (ALP) is an early differentiation marker associated with calcification. Therefore, osteogenesis can be demonstrated by the expression of ALP. BMSCs were cultivated on a 24-well cell culture plate, which had ligaments preset inside it, with density as $5.3ith^3$ cell/cm^2. We transferred the samples to new culture plates after 8 hours of culture. After 14 days of culture, both cells and upper supernatant of cultivating suspension were collected for determining ALP activity in intercellular and extracellular environment respectively. ALP activity was measured in triplicate with a rabbit ALP ELISA kit (E-EL-RB0022; Elabscience, Wuhan, Hubei, China).

Integrin β1 of supernatant was measured in BMSCs using commercial enzyme immunoassay kits (DYC3230E; R&D Systems, Minneapolis, MN ,USA) in accordance with the manufacturer's instructions. BMSCs (1.1×0.1^4 cell/cm^2) were seeded in 24-well plates, which had ligaments preset inside it, containing DMEM supplemented with 10% fetal bovine serum. After 8 hours of culture, we transferred the samples to new culture plates for the following experiment. After 3 days of culture, both cells and upper supernatant of cultivating suspension were collected for determining expression level of integrin β1.

Animal study design and surgical procedure

All animal experiments were approved by the Institutional Animal Care and Use Committee at Fudan University for the care and use of laboratory animals. Animal surgical procedure was undertaken as previously described.[14–16] Briefly, 72 mature male New Zealand rabbits (mean weight 2.8±0.5 kg) were randomly divided into three groups: PET group, PET+SF group, and PET+SF+HAP group. All these animals underwent extra-articular graft-to-bone surgery

procedure. Among them, 36 New Zealand rabbits were used for mechanical testing, and the other ones were used for histological examination. All rabbits were anesthetized with 3% pentobarbital (30 mg/kg). After skin disinfection and incision, a 3 mm diameter bone tunnel was drilled in the proximal tibial metaphysis. The legs of the rabbits were randomly divided into the experimental side and the control side. The SF-coated graft (PET+SF or PET+SF+HAP) was pulled into one leg as the experimental group, while the PET graft was implanted into the contralateral leg as the control group. An almost 0.5 cm long graft was left outside the lateral tunnel entrance for the subsequent biomechanical test. The graft end was sutured with the adjacent periosteum and soft tissue at the tunnel entrance, and then the wound was closed layer by layer. Postoperatively, the animals were returned to the cages and allowed to move freely in the cages without immobilization. Buprenorphine (0.05 mg/kg) was used subcutaneously for pain control for 3 days. These rabbits were sacrificed 4 and 8 weeks after surgery for the subsequent tests.

Mechanical testing

Each rabbit from each group (n=12) was sacrificed either 4 (n=6) or 8 (n=6) weeks postoperatively, and the graft-tibia complex prepared immediately for mechanical test without being frozen. All scar tissues and sutures were carefully removed from the tibial tunnel exits. Mechanical test was conducted using an Instron materials testing system machine (8,874; Instron Co., Norwood, MA, USA) according to established procedures by former researchers.[14–16] The graft end outside of the lateral tunnel entrance was sutured by a No 5 Ethibond suture for drawing, and the tibial portion was fixed firmly by a clamp. The bone tunnel was oriented parallel with the testing axis. Before the tensile test, the samples were preloaded with a static preload of 1 N for 5 minutes. After preconditioning, the ultimate failure load was carried out immediately with an elongation rate of 2 mm/min. The load–deformation curve was recorded, from which the ultimate failure load (N) was measured. Stiffness (N/mm) was calculated from the slope of the linear region of the load–deformation curve at the maximal load-to-failure point. For each sample, the test was completed when the graft was ruptured or pulled out of the bone tunnel.

Histological examination

To reflect the bone-tendon healing process of the graft-tibia complexes by the histological examination, the graft-tibia complexes were harvested in each group (n=6) respectively 4 and 8 weeks postoperatively. After being sacrificed, the graft-bone complex samples were fixed in 10% formalin for 48 hours, and then embedded, undecalcified in a methyl methacrylate compound. The samples were sectioned perpendicularly to the longitudinal axis of the tibial tunnel with a thickness of 5 μm by using a microtome (SM2500; Leica, Nussloch, Germany). These sections were stained with hematoxylin and eosin (H&E), and Masson trichrome stain was also performed for routine light microscopic examination. The slides were examined to visualize the graft–bone interface with inverted light microscopy (IX71SBF-2; Olympus Optical Co., Tokyo, Japan), and the digital images were taken using a DP Manager (Olympus Optical Co., Tokyo, Japan). The two investigators performing the histological analysis were blinded to the animal surgery.

Histomorphometric analysis

The histomorphometric analysis was based on the finding of H&E staining. Each section taken at the middle portion of the tunnel was divided into four quadrants to determine the width of the graft–bone interface. In each of the four quadrants, the width of the graft–bone interface was measured as the distance between the edge of the bone tunnel and the outer graft determined under ×200 magnification. Four separate measurements were conducted in each of the quadrants for a total of 16 measurements for each sample. Then, the average width of the graft–bone interfaces was calculated in each sample. Histomorphometric analyzers were blinded to the animal surgery in this procedure.

Real-time polymerase chain reaction (RT-PCR) analysis

The graft–tibia complex (n=6 limbs in each group 4 or 8 weeks postoperatively) was harvested from each knee after sacrifice for RT-PCR analysis, respectively. Total RNA from interfacial samples between host bone tunnel and graft were extracted using TRIzol reagent (Invitrogen, Carlsbad, CA, USA) based on the manufacturer's instructions. The cDNA was generated using reverse-transcriptase M-MLV (D2640A; Takara, Beijing, People's Republic of China) according to the manufacturer's protocol. Quantitative PCR was performed with SYBR Premix Ex Taq (DRR041A; Takara), and then detected by a real-time PCR system (TP800; Takara, Kyoto, Japan).

cDNA from 200 ng total RNA was used as the template. The PCR reaction was carried out under the following conditions: 40 cycles of denaturation at 95°C for 10 seconds, annealing at 60°C for 20 seconds, and extension at 72°C for

20 seconds. The mRNA levels of *BMP-7* and vascular endothelial growth factor (*VEGF*) were normalized to the expression of an endogenous housekeeping gene, *β-actin*, using the delta-delta Ct method. The primers for RT-PCR were described as follows: for *β-actin* (NM_001101683.1), forward 5′-CAA CCG CGA GAA GAT GAC CC-3′ and reverse 5′-TAG CCC TCG TAG ATG GGC ACC GT-3′; for *BMP-7* (EU004072.1), forward 5′-GAGTGCGCCTTCCCCCTCAA-3′ and reverse 5′-AACTGTCGTCGAAGTAGAGGA-3′; for *VEGF* (AY196796.1), forward 5′-GACAATAAACCCCA CGAAGT-3′ and reverse 5′-TTCATCATTGCAGCAG CCCCCACA-3′. The lengths of amplified products were 165 bp, 154 bp, and 171 bp.

Statistical analysis

Data analysis was performed using SPSS for Windows, release 13.0.0 (SPSS Inc., Chicago, IL, USA) statistical software and reported as mean and standard deviation for description. The data were compared between the control and experimental limbs using a paired Student's *t*-test. Comparisons of groups at different time points were performed using an independent two-sample Student's *t*-test. Comparisons of numerical data among multiple groups were performed by one-way analysis of variance (ANOVA), least significant difference (LSD) *t*-test. All *P*-values were two-sided, and a *P*-value of <0.05 was considered statistically significant.

Results

Morphology of ligaments

Results of SEM observation on the three kinds of ligaments are shown in Figure 1A–C. It was found that the surface of the PET fiber in the artificial ligament was smooth even after plasma pretreatment. SF coating on the PET ligament brought lots of bead-like particles to the surface and changed the even surface into a convex one. After the biomineralization process, HAP particles were deposited uniformly on the surface of the fiber and formed a shell wrapping all over the fiber. In order to obtain more detailed information on the surface of the three kinds of ligaments, AFM observation in tapping model was executed further. The results are presented in Figure 1D–F. Information revealed from three-dimensional topography of ligaments acquired by AFM was consistent with those obtained by SEM. PET fiber after plasma treatment had a flatter surface than the other two samples, and only few convex regions were found in the PET topography. PET+SF presented much more bumpy topography, and the PET+SF+HAP group displayed a zigzag one. It means both the coating of SF and deposition of HAP significantly changed the external morphology of the ligaments by refining the roughness of the surface. Therefore, the modification using a novel coating technique of the ligament surface is helpful to osseointegration in the bone tunnel by increasing adhesion of BMSCs.[31]

Characterization of ligaments

ATR-FTIR was utilized to investigate the molecular interactions of chemical components at the surface of the ligaments. It can be seen in Figure 2 that the PET ligament displayed a typical PET FTIR spectrum, in which 1,025 cm^{-1} is assigned to =CH bending vibration in-plane of benzene, 1,107 cm^{-1} to C-O-C symmetric stretching vibration, 1,271 cm^{-1} to C-O asymmetric stretching vibration, 1,435 cm^{-1} to C=C stretching vibration of benzene, and 1,720 cm^{-1} to -C=O stretching vibration.[32] When SF was immobilized on to PET surface through coating method, absorption bands at 1,623 cm^{-1} (assigned to amide I of SF β-sheet structure) and 1,520 cm^{-1} (assigned to the amide II of SF β-sheet structures) showed up (Figure 2), indicating the successful introduction of SF onto the PET surface.[33] A strong peak at 1,050 cm^{-1} in the FTIR spectrum of PET+SF+HAP was indicative of the ν3 vibrations of PO_4^{3-}.[34] Meanwhile, those typical absorption bands of PET and SF became weaker and even disappeared. It meant signals emitted by PET and SF in the ATR-FTIR test were blocked by HAP when the fiber in the ligament was wrapped by the depositing HAP after the biomineralization process.

The chemical composition of the ligaments was further investigated by EDX, and Figure 3A represents a typical spectrum corresponding to the depositing inorganic crust of PET+SF+HAP in Figure 1C. The Ca/P ratio in the inorganic layer was 1.52±0.07 (an average result of six measurements), a little bit smaller than 1.67 of the standard HAP. XRD was able to clarify ordered structure of materials, and then information including crystal type, distance between lattice, and crystallinity could be collectedly simultaneously. Figure 3B displays a representative XRD pattern of the PET+SF+HAP group. Typical diffraction peaks of PET appeared at 17.8°, 23°, 26.2°, and 43.8°, standing for lattice [111], [110], [100], and [101], respectively. Peaks at 2θ=26.2°, 32.1°, 32.7°, 34.3°, 39.7°, 46.9°, 49.6°, and 53.6° were clearly characteristic of HAP crystals.[34] However, these peaks were broadened in the PET+SF+HAP group as compared with those of pure HAP in reported literature, indicating a relative poor crystallinity, which might be induced by the disorder in the crystal, such as the substitution of HPO_4^{2-} and CO_3^{2-} for PO_4^{3-}, or Na^+

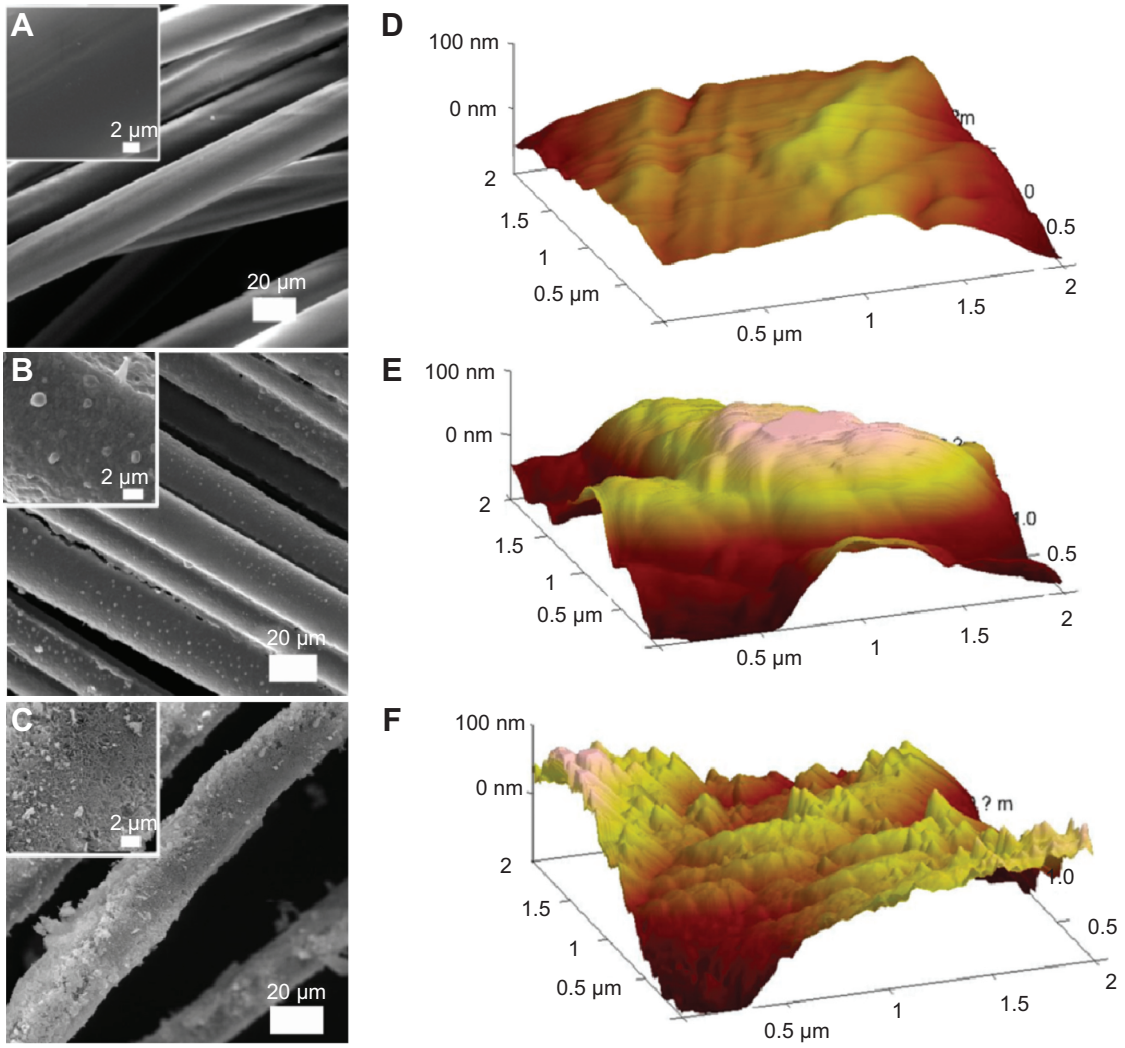

Figure 1 Scanning electron microscopy observation of PET (**A**), PET+SF (**B**), and PET+SF+HAP (**C**); inset pictures are amplified. Three-dimensional topography of PET (**D**), PET+SF (**E**), and PET+SF+HAP (**F**), acquired by atomic force microscopy in tapping mode.
Abbreviations: HAP, hydroxyapatite; PET, polyethylene terephthalate; SF, silk fibroin.

for Ca^{2+}.[34] We also noticed that the peak at 26.2° might be related to other calcium phosphate, such as DCPA (dimethyl tetrachloroterephthalate). Therefore, it was possible that more than one kind of calcium phosphate formed through the biomineralization route and deposited on the ligament.

Cell proliferation, differentiation, and adhesion

As shown in Figure 4A, BMSC proliferation in the PET+SF+HAP group was found to be better than the PET group and PET+SF group in CCK-8 assay from 24 to 120 hours. Moreover, statistical analysis indicated that the difference of living cell number after 5 days cultivation between the PET+SF+HAP group and the PET group was significant at 0.01 level, and so was the difference between the PET+SF group and the PET group ($P<0.01$).

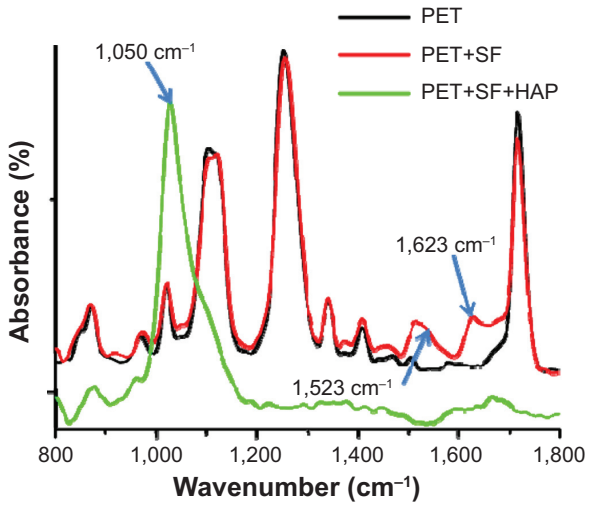

Figure 2 ATR-FTIR spectrum of three kinds of ligaments sample.
Abbreviations: ATR-FTIR, attenuated total reflectance Fourier transform infrared; HAP, hydroxyapatite; PET, polyethylene terephthalate; SF, silk fibroin.

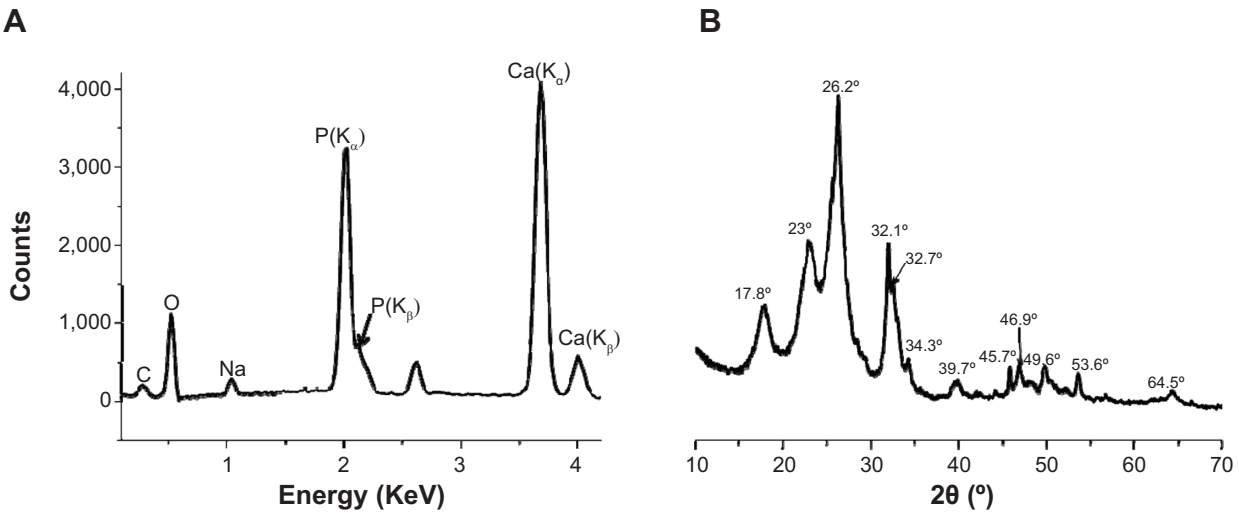

Figure 3 Energy-dispersive X-ray spectrum (**A**) and X-ray diffraction pattern (**B**) of PET+SF+HAP.
Abbreviations: HAP, hydroxyapatite; PET, polyethylene terephthalate; SF, silk fibroin.

Cellular differentiation was measured by evaluating the ALP activity, both extracellularly and intercellularly. Figure 4B shows the results of the ALP activity for all samples. After 14 days of culture, the cells in the PET+SF+HAP group delivered a much higher level of ALP activity than in the other two groups, and the differences were significant at the 0.05 level for extracellular and at 0.01 for intercellular. However, the differences between the PET group and the PET+SF group were insignificant, though the activity of ALP in the PET+SF group was higher than in the PET group ($P<0.05$).

Cell adhesion was assessed by measuring the expression level of integrin β1 (Figure 4C). After 3 days of culture, the PET+SF+HAP group and the PET+SF group were higher than the PET group (both $P<0.01$). No significant difference was observed between the PET+SF+HAP group and the PET+SF group ($P>0.05$).

Mechanical findings

Regardless of the implantation duration (4 or 8 weeks), all samples failed when they were pulled out from the bone tunnel.

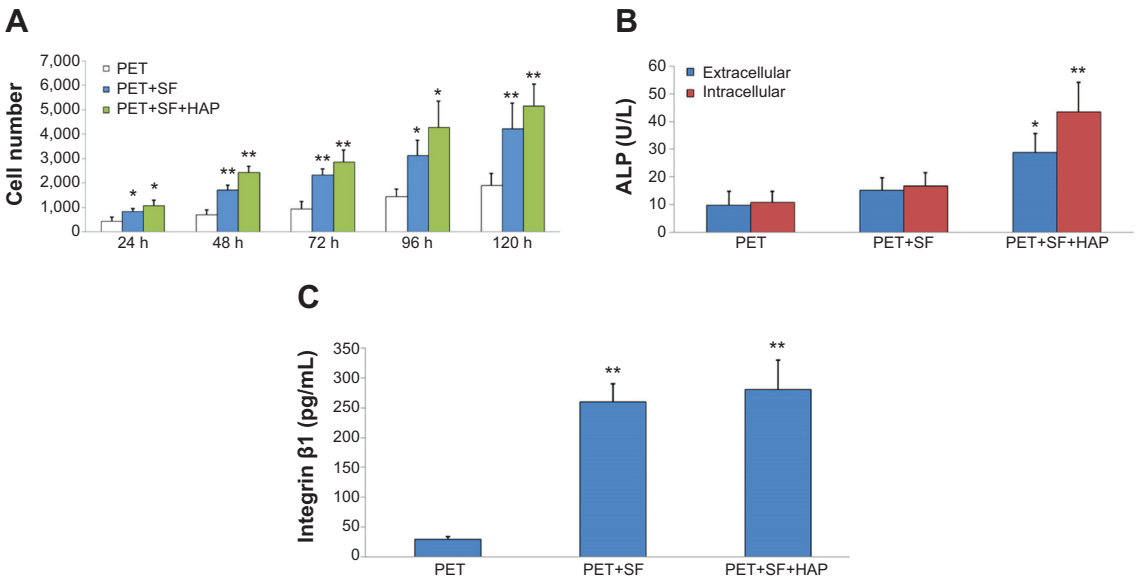

Figure 4 Measurement of BMSC proliferation, differentiation, and adhesion among the PET group, PET+SF group, and PET+SF+HAP group.
Notes: (**A**) BMSC proliferation was measured by CCK-8 assays. (**B**) Cell differentiation was monitored by measuring the ALP activity. (**C**) Cell adhesion was assessed by measuring the expression level of integrin β1. *$P<0.05$; **$P<0.01$.
Abbreviations: ALP, alkaline phosphatase; BMSC, bone marrow stromal cell; CCK, cell counting kit; HAP, hydroxyapatite; PET, polyethylene terephthalate; SF, silk fibroin.

No PET grafts were ruptured. At the 4th week after surgery, there was no statistically significant difference in the load to failure among the PET group (38.80±5.12 N), PET+SF group (40.60±5.18 N), and PET+SF+HAP group (44.40±8.26 N) (P=0.393, one-way ANOVA). At the 8th week after surgery, the mean load to failure of the PET+SF+HAP group (91.00±5.39 N) was higher than those of the PET group (56.60±5.37 N) (P=0.000, LSD t-test) and the PET+SF group (62.80±5.59 N) (P=0.000, LSD t-test) (Figure 5A). Likewise, at the 4th week after surgery, there was no statistically significant difference in the stiffness value among the PET group (4.00±1.70 N/mm), PET+SF group (4.80±1.20 N/mm), and PET+SF+HAP group (5.20±1.48 N/mm) (P=0.448, one-way ANOVA). At the 8th week after surgery, the stiffness value of the PET+SF+HAP group (8.10±1.78 N/mm) was higher than those of the PET group (5.20±0.84 N/mm) (P=0.004, LSD t-test) and the PET+SF group (6.00±1.00 N/mm) (P=0.023, LSD t-test) (Figure 5B).

Histological findings

In the PET group and the PET+SF group, thick fibrous scar tissue was formed at the graft-to-bone interface 4 and 8 weeks after surgery. No obvious new bone formation was observed in either the PET group or the PET+SF group. In the PET+SF+HAP group, thick fibrous scar tissue was also found at the graft-to-bone interface 4 weeks after surgery. While 8 weeks after surgery, some protruding new bone tissue formation was found at the interface between host bone and graft. Furthermore, the interface width became much narrower, and there was less fibrous tissue formation in the PET+SF+HAP group (Figure 6).

Findings of Masson staining

In the PET group and the PET+SF group, collagen fibers moderately formed and infiltrated into the PET graft 4 and 8 weeks after surgery. While in the PET+SF+HAP group 8 weeks after surgery, there were more collagen fibers formed, and the PET fibers were almost completely encircled by collagen (light blue stained), and neoformative bone tissue protruding into the interface of the graft and host bone was observed (as indicated by black arrows in Figure 7F). However, the orientations of the newly formed collagen fibers in the three groups were not orderly enough (Figure 7).

Histomorphometric analysis

Histomorphometric analysis showed that the graft–bone interface width in PET+SF+HAP group (277.81±41.34 μm) was narrower than those in the PET group (315.00±51.75 μm) (P=0.038, LSD t-test) and PET+SF group (308.19±43.86 μm) (P=0.042, LSD t-test) at the 4th week after surgery. Subsequently, at the 8th week after surgery, there was much more difference in the graft–bone interface width among these three groups. The graft–bone interface width of the PET+SF+HAP group (139.19±38.96 μm) was significantly narrower than those of the PET group (219.38±47.59 μm) (P=0.000, LSD t-test) and PET+SF group (207.12±44.49 μm) (P=0.000, LSD t-test). However, no significant differences were confirmed between the PET group and the PET+SF group (P>0.05, LSD t-test) (Figure 8).

RT-PCR

The mRNA expression level of *BMP-7* in the PET+SF+HAP group (0.79±0.11) was significantly higher than those in

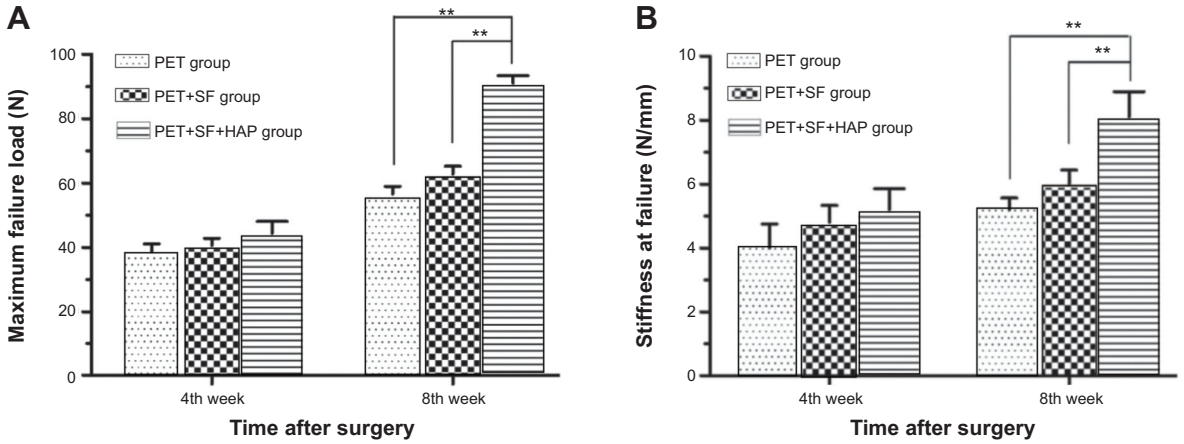

Figure 5 Mechanical examinations for graft–bone healing in a rabbit model at each time point after surgery.
Notes: (**A**) Comparison of maximal failure load among the PET group, PET+SF group, and SF+HAP group. (**B**) Comparison of stiffness at failure among the PET group, PET+SF group, and PET+SF+HAP group. **P<0.01.
Abbreviations: HAP, hydroxyapatite; PET, polyethylene terephthalate; SF, silk fibroin.

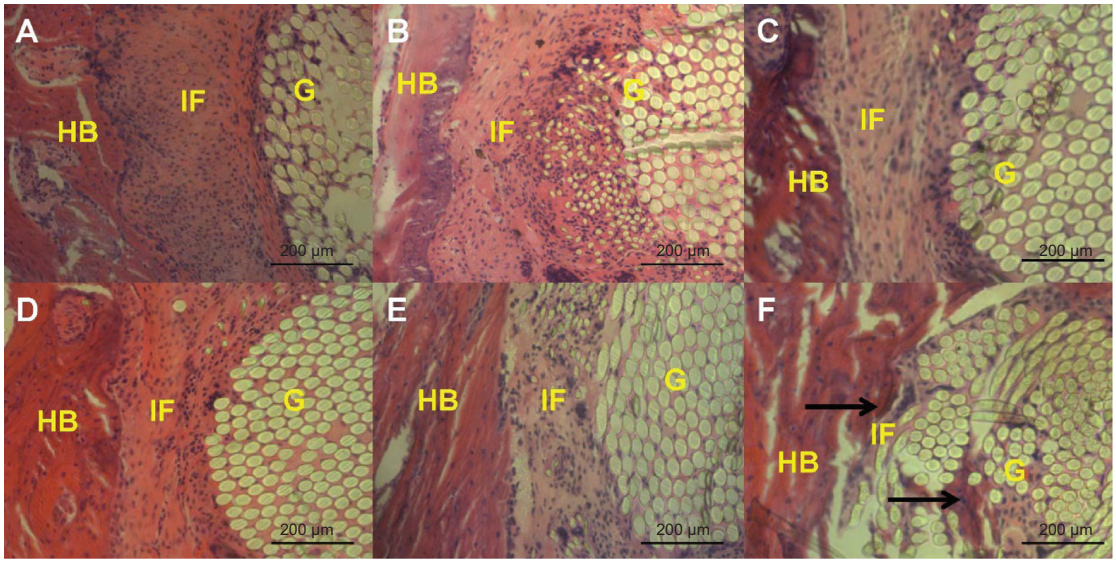

Figure 6 Histological characterization of the PET group (**A** and **D**), PET+SF group (**B** and **E**), and PET+SF+HAP group (**C** and **F**) at 4 weeks (**A**, **B**, and **C**) and 8 weeks (**D**, **E**, and **F**) after surgery.
Notes: The figure shows the interface between the host bone and the graft (H&E staining, ×200 magnification). In the PET+SF+HAP group 8 weeks after surgery, new bone growth into the interface was observed (as indicated by black arrows). Bar =200 μm.
Abbreviations: G, artificial ligament graft; H&E, hematoxylin and eosin; HAP, hydroxyapatite; HB, host bone; IF, interface; PET, polyethylene terephthalate; SF, silk fibroin.

the PET group (0.44±0.07) (P=0.000, LSD t-test) and the PET+SF group (0.47±0.08) (P=0.000, LSD t-test) at the 4th week after surgery. At the 8th week after surgery, the mRNA expression level of *BMP-7* in the PET+SF+HAP group (0.62±0.10) was also higher than those in the PET group (0.30±0.14) (P=0.001, LSD t-test) and the PET+SF group (0.38±0.11) (P=0.005, LSD t-test). However, there were no significant differences of the mRNA expression level of *VEGF* among the PET group, PET+SF group and PET+SF+HAP group at the 4th week (0.44±0.08 versus 0.47±0.08 versus 0.54±0.07; P=0.158, one-way ANOVA) and 8th week (0.40±0.07 versus 0.43±0.07

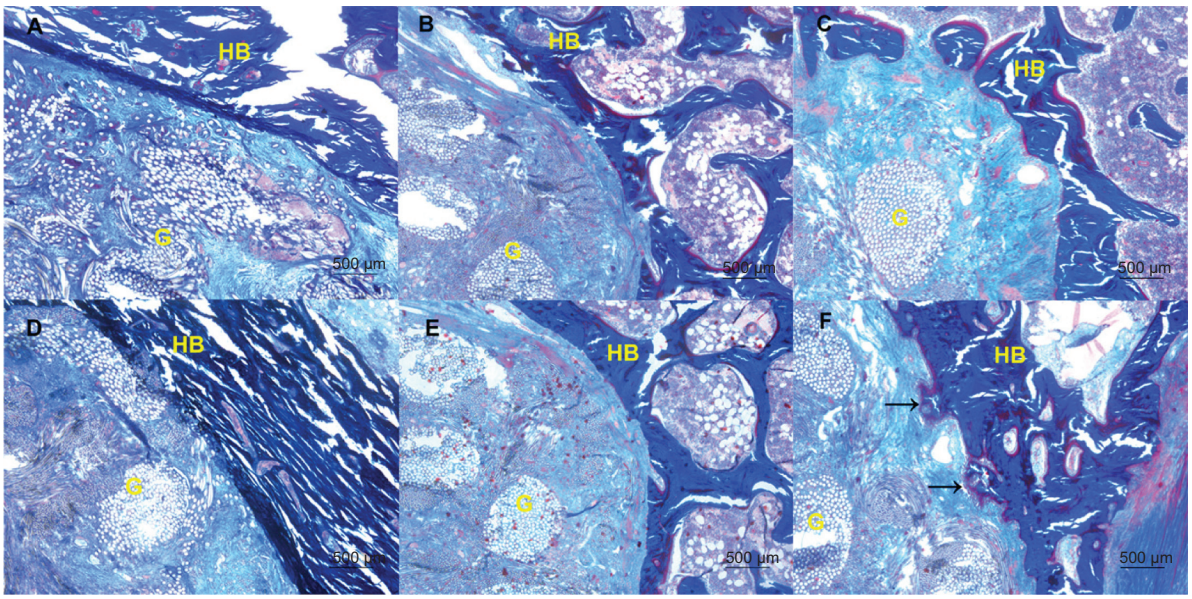

Figure 7 Collagen fiber status of the PET group (**A** and **D**), PET+SF group (**B** and **E**), and PET+SF+HAP group (**C** and **F**) at 4 weeks (**A**, **B**, and **C**) and 8 weeks (**D**, **E**, and **F**) after surgery.
Notes: The figure shows the formation and infiltration of the collagen fibers and bone formation at the interface of the graft and the host bone (Masson staining, ×40 magnification). In the PET+SF+HAP group 8 weeks after surgery, plenty of collagen fibers and new bone (as indicated by black arrows) was found. Bar =500 μm.
Abbreviations: G, artificial ligament graft; HAP, hydroxyapatite; HB, host bone; PET, polyethylene terephthalate; SF, silk fibroin.

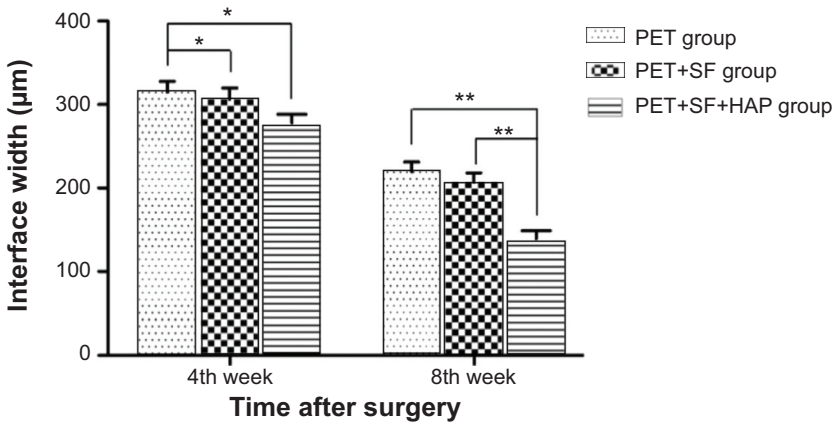

Figure 8 Interface width between the host bone and the graft of the PET group, PET+SF group, and PET+SF+HAP group 4 and 8 weeks after surgery.
Notes: *$P<0.05$; **$P<0.01$.
Abbreviations: HAP, hydroxyapatite; PET, polyethylene terephthalate; SF, silk fibroin.

versus 0.47±0.05; $P=0.204$, one-way ANOVA) after surgery (Figure 9).

Discussion

The choosing of graft in the reconstruction of ACL has always been the focus of attention in sports medicine.[35] In the last decade, the artificial ligament made of PET was deemed the best choice of artificial ligament in the reconstruction procedure for its relatively good histocompatibility and outstanding mechanical property, with the LARS artificial ligament being a well-known representation in the market.[11]

However, the long-term effect of the PET artificial ligaments is a disputable issue.[36] The aspect centering on the graft–bone healing process is the main topic in this issue. As we have already found in the previous research, being a hydrophobic material with chemical inertness, the PET advocates were convinced that this substitute was of a low tissue-inductive capability and poor cell-adhesive function.[14–16] Now we believe that the work modifying the surface of the PET will cover the shortages. Meanwhile in this field, works targeting on the graft–bone healing process of a PET substitute are given top priority.

We have testified that the method in which the HAP was directly coated on the PET could effectively enhance the differentiation of osteoblast in vitro.[15] Although the results of in vitro research are encouraging, poor graft–bone healing results in an in vivo study reminded us that the uneven coating on the PET had hindered the healing process. SF is a kind of animal protein void of physiological activity; the implantation of such material in animal models does not lead to an allergic reaction thanks to its property of non-antigen and total degradability.[22,37] In addition, SF has a relatively ideal mechanical strength, which wins itself an important role in tissue-repair work, especially in the repair of bone defects using composite material prepared by SF-inductive biomimetic mineralization.[34] Based on the characteristics of SF, we have tried to prepare PET with a coating of SF, which would present a reasonable inductive surface for the

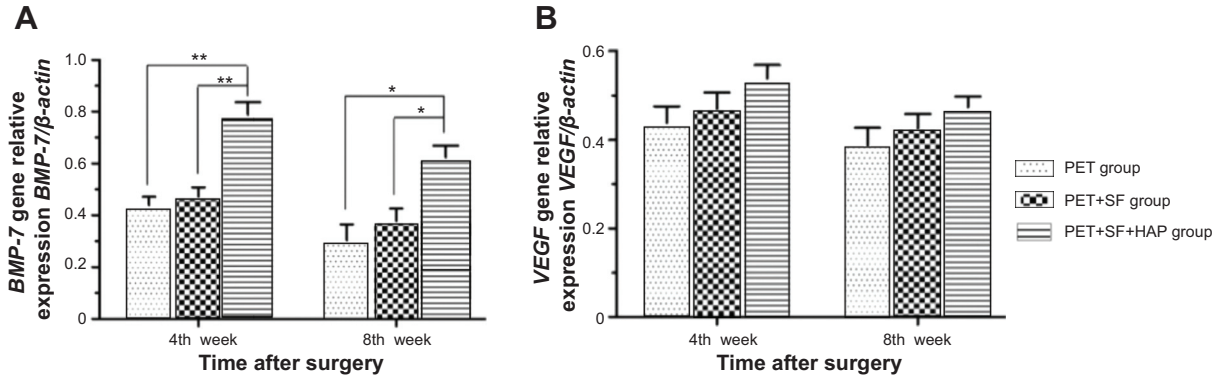

Figure 9 RT-PCR analysis shows mRNA expression levels of *BMP-7* (**A**) and *VEGF* (**B**) 4 and 8 weeks after surgery.
Notes: *$P<0.05$; **$P<0.01$.
Abbreviations: mRNA, messenger RNA; RT-PCR, real-time polymerase chain reaction; *VEGF*, vascular endothelial growth factor.

further biomimetic mineralization of the HAP. This procedure was performed to maximally mirror the natural process of biogenic deposit, which will enable the construction of a microenvironment for native osteogenesis and effectively promote the bone formation progress.

After the SF-coating preparation and subsequent biomimetic mineralization, SEM, AFM, ATR-FTIR, and EDX were adopted to illustrate the details of SF-coating and HAP deposit. In vitro study, the cell proliferation using CCK-8, the ALP activity, and the expression of integrin β1 in the PET+SF+HAP group were all higher than in the other groups at 8 weeks, and the differences among groups were significant in statistical analysis, which confirmed its efficacy in cellular conductivity and osteogenic process. Compared with the PET+SF group, which had no significant elevation in ALP activity, the PET+SF+HAP group showed a promising result due to the natural osteogenic and osteoconductive potential of HAP that is widely applied in bone and dental repair materials. This study matched our previous one of HAP/regenerated SF scaffold preparation for enhanced osteoinductivity and osteoconductivity that could be concluded as osteointegration.[38]

In in vivo study, the PET+SF+HAP group demonstrated the best mechanical properties among all trial groups in the pull-out experiment of graft–bone composite. Meanwhile, H&E staining in histologic study demonstrated that compared with the other groups in which all graft–bone surfaces were covered with thick scar tissue, the PET+SF+HAP group had a narrower bone–graft interface with less cicatrix tissue. By Masson staining, the formation of new bone and its penetration of the interface of graft–bone toward the inner part of the graft had been confirmed in the PET+SF+HAP group. The RNA expression of *VEGF* in the PET+SF+HAP group was higher than in the other two groups, while it was higher in the PET+SF group than in the PET group. However, these differences were not statistically significant, which suggested our coating had limited potential for neovascularization. Lastly, the RNA expression of *BMP-7* in the PET+SF+HAP group was significantly higher than in the other groups, which again proved the osteoinduction capacity to promote osteogenesis in the PET+SF+HAP group.

Compared with those methods of surface coating using the HAP or the bioglass for the PET refining process in earlier reports,[14–16] the biomimetic mineralization adopting the SF and the HAP showed a more favorable efficacy to those former ones. We found a narrowing interface of the graft–bone and penetration of surrounding tissue into the grafts. More significantly, the subsequent in-growth of new bone into the graft has been observed during research, which underlines the method to be qualified as a more effective method in PET preparation for graft–bone healing capacity enhancement.[39] Above all, the SF+HAP coating prepared by biomimetic mineralization on the surface of PET possesses the benefits of simplicity in manufacturing, high cellular and tissue induction, and also effective osteogenesis facilitation. Its osteoinduction and osteoconduction are better than traditional materials by creating a relatively more natural microenvironment during the bone-formation process. To meet the strict standards of artificial synthesis for clinical usage in an industrialization route, further research will be centered on refining the process, consisting of more elaborate steps and animal experiments using large animals.

Acknowledgments

We are grateful to the staff in the Key Laboratory of Molecular Engineering of Polymers of Ministry of Education, Department of Macromolecular Science, and Laboratory of Advanced Materials, Fudan University. This work was supported by the Grants from the Projects of National Natural Science Foundation of China (No. 81271958 and No. 81370052), Specialized Research Fund for the Doctoral Program of Higher Education (NO.20120071110067) and the Project of Shanghai Municipal Science and Technology Commission (11JC1401700).

Disclosure

The authors declare that they have no competing interests.

References

1. Cooper JA, Sahota JS, Gorum WJ, Carter J, Doty SB, Laurencin CT. Biomimetic tissue-engineered anterior cruciate ligament replacement. *Proc Natl Acad Sci U S A.* 2007;104(9):3049–3054.
2. Guarino V, Causa F, Ambrosio L. Bioactive scaffolds for bone and ligament tissue. *Expert Rev Med Devices.* 2007;4(3):405–418.
3. Harner CD, Giffin JR, Dunteman RC, Annunziata CC, Friedman MJ. Evaluation and treatment of recurrent instability after anterior cruciate ligament reconstruction. *Instr Course Lect.* 2001;50:463–474.
4. Heath CA, Rutkowski GE. The development of bioartificial nerve grafts for peripheral-nerve regeneration. *Trends Biotechnol.* 1998;16(4):163–168.
5. Brunelli GA, Battiston B, Vigasio A, Brunelli G, Marocolo D. Bridging nerve defects with combined skeletal muscle and vein conduits. *Microsurgery.* 1993;14(4):247–251.
6. Milthorpe BK. Xenografts for tendon and ligament repair. *Biomaterials.* 1994;15(10):745–752.
7. Cartmell JS, Dunn MG. Development of cell-seeded patellar tendon allografts for anterior cruciate ligament reconstruction. *Tissue Eng.* 2004;10(7–8):1065–1075.
8. Sterling JC, Meyers MC, Calvo RD. Allograft failure in cruciate ligament reconstruction. Follow-up evaluation of eighteen patients. *Am J Sports Med.* 1995;23(2):173–178.

9. Olson EJ, Kang JD, Fu FH, Georgescu HI, Mason GC, Evans CH. The biochemical and histological effects of artificial ligament wear particles: in vitro and in vivo studies. *Am J Sports Med.* 1988;16(6):558–570.
10. Lavoie P, Fletcher J, Duval N. Patient satisfaction needs as related to knee stability and objective findings after ACL reconstruction using the LARS artificial ligament. *Knee.* 2000;7(3):157–163.
11. Gao K, Chen S, Wang L, et al. Anterior cruciate ligament reconstruction with LARS artificial ligament: a multicenter study with 3- to 5-year follow-up. *Arthroscopy.* 2010;26(4):515–523.
12. Guidoin M-F, Marois Y, Bejui J, Poddevin N, King MW, Guidoin R. Analysis of retrieved polymer fiber based replacements for the ACL. *Biomaterials.* 2000;21(23):2461–2474.
13. Mei-Dan O, Mann G, Steinbacher G, Ballester S, Cugat R, Alvarez P. Septic arthritis with Staphylococcus lugdunensis following arthroscopic ACL revision with BPTB allograft. *Knee Surg Sports Traumatol Arthrosc.* 2008;16(1):15–18.
14. Li H, Wu Y, Ge Y, et al. Composite coating of 58S bioglass and hydroxyapatite on a poly (ethylene terepthalate) artificial ligament graft for the graft osseointegration in a bone tunnel. *Appl Surf Sci.* 2011;257(22):9371–9376.
15. Li H, Ge Y, Wu Y, et al. Hydroxyapatite coating enhances polyethylene terephthalate artificial ligament graft osseointegration in the bone tunnel. *Int Orthop.* 2011;35(10):1561–1567.
16. Li H, Chen S, Wu Y, et al. Enhancement of the osseointegration of a polyethylene terephthalate artificial ligament graft in a bone tunnel using 58S bioglass. *Int Orthop.* 2012;36(1):191–197.
17. Altman GH, Diaz F, Jakuba C, et al. Silk-based biomaterials. *Biomaterials.* 2003;24(3):401–416.
18. Jin H-J, Chen J, Karageorgiou V, Altman GH, Kaplan DL. Human bone marrow stromal cell responses on electrospun silk fibroin mats. *Biomaterials.* 2004;25(6):1039–1047.
19. Fare S, Torricelli P, Giavaresi G, et al. In vitro study on silk fibroin textile structure for Anterior Cruciate Ligament regeneration. *Mater Sci Eng C Mater Biol Appl.* 2013;33(7):3601–3608.
20. Freed LE, Vunjak-Novakovic G, Biron RJ, et al. Biodegradable polymer scaffolds for tissue engineering. *Nat Biotech.* 1994;12(7):689–693.
21. Zhou G, Shao Z, Knight DP, Yan J, Chen X. Silk fibers extruded artificially from aqueous solutions of regenerated Bombyx mori silk fibroin are tougher than their natural counterparts. *Adv Mater.* 2009;21(3):366–370.
22. Rockwood DN, Preda RC, Yücel T, Wang X, Lovett ML, Kaplan DL. Materials fabrication from Bombyx mori silk fibroin. *Nat Protoc.* 2011;6(10):1611–1631.
23. Lv Q, Zhang X, Hu X, Kaplan DL. Green process to prepare silk fibroin/gelatin biomaterial scaffolds. *Macromol Biosci.* 2010;10:289–298.
24. Wei GJ, Yao M, Wang YS, et al. Promotion of peripheral nerve regeneration of a peptide compound hydrogel scaffold. *Int J Nanomedicine.* 2013;8:3217–3225.
25. Zhu Y, Chen Y, Xu G, Ye X, He D, Zhong J. Micropattern of nano-hydroxyapatite/silk fibroin composite onto Ti alloy surface via template-assisted electrostatic spray deposition. *Mater Sci Eng C.* 2012;32(2):390–394.
26. Wang L, Ning G-L, Senna M. Microstructure and gelation behavior of hydroxyapatite-based nanocomposite sol containing chemically modified silk fibroin. *Colloids Surf A Physicochem Eng Asp.* 2005;254(1–3):159–164.
27. Qian J, Suo A, Jin X, Xu W, Xu M. Preparation and in vitro characterization of biomorphic silk fibroin scaffolds for bone tissue engineering. *J Biomed Mater Res A.* 2014;102(9):2961–2971.
28. Wang H, Li Y, Zuo Y, Li J, Ma S, Cheng L. Biocompatibility and osteogenesis of biomimetic nano-hydroxyapatite/polyamide composite scaffolds for bone tissue engineering. *Biomaterials.* 2007;28(22):3338–3348.
29. Shao XX, Hutmacher DW, Ho ST, Goh JCH, Lee EH. Evaluation of a hybrid scaffold/cell construct in repair of high-load-bearing osteochondral defects in rabbits. *Biomaterials.* 2006;27(7):1071–1080.
30. Ye ZL, Hou XX, Chen RL, et al. Effects of methylthiouracil on the proliferation and apoptosis of rat bone marrow stromal cells. *Exp Ther Med.* 2014;7(6):1738–1744.
31. Yao X, Peng R, Ding J. Cell-material interactions revealed via material techniques of surface patterning. *Adv Mater.* 2013;25(37):5257–5286.
32. Kamlendra Awasthi, Vaibhav Kulshrestha, Avasthi DK, Vijay YK. Optical, chemical and structural modification of oxygen irradiated PET. *Radiat Meas.* 2010;45:850–855.
33. Chen X, Shao ZZ, Marinkovic NS, Miller LM, Zhou P, Chance MR. Conformation transition kinetics of regenerated Bombyx mori silk fibroin membrane monitored by time-resolved FTIR spectroscopy. *Biophys Chem.* 2001;89(1):25–34.
34. Cao H, Chen X, Shao ZZ. Preparation of hydroxyapatite/silk fibroin electrospun fibers and their application to mineralization. *Acta Chimica Sinica.* 2008;66(18):2059–2064.
35. Kimura Y, Hokugo A, Takamoto T, Tabata Y, Kurosawa H. Regeneration of anterior cruciate ligament by biodegradable scaffold combined with local controlled release of basic fibroblast growth factor and collagen wrapping. *Tissue Eng Part C Methods.* 2008;14(1):47–57.
36. Glezos CM, Waller A, Bourke HE, Salmon LJ, Pinczewski LA. Disabling synovitis associated with LARS artificial ligament use in anterior cruciate ligament reconstruction: a case report. *Am J Sports Med.* 2012;40(5):1167–1171.
37. Veparia C, Kaplan DL. Silk as a biomaterial. *Prog Polym Sci.* 2007;32:991–1007.
38. Jiang J, Hao W, Li Y, et al. Hydroxyapatite/regenerated silk fibroin scaffold-enhanced osteoinductivity and osteoconductivity of bone marrow-derived mesenchymal stromal cells. *Biotechnol Lett.* 2013;35(4):657–661.
39. Mulford JS, Chen D. Anterior cruciate ligament reconstruction: a systematic review of polyethylene terephthalate grafts. *ANZ J Surg.* 2011;81(11):785–789.